Effect of Mn doping on the structural and optical properties of sol–gel derived ZnO nanoparticles

Article *in* Central European Journal of Physics · April 2011

DOI: 10.2478/s11534-011-0106-4

3 authors:

Abdub Guyo Ali
University of the Free State
6 PUBLICATIONS **19** CITATIONS
SEE PROFILE

F. B. Dejene
University of the Free State
94 PUBLICATIONS **331** CITATIONS
SEE PROFILE

H. C. Swart
University of the Free State
528 PUBLICATIONS **3,327** CITATIONS
SEE PROFILE

Cent. Eur. J. Phys. • 10(2) • 2012 • 478-484
DOI: 10.2478/s11534-011-0106-4

VERSITA

Central European Journal of **Physics**

Effect of Mn doping on the structural and optical properties of sol-gel derived ZnO nanoparticles

Research Article

Abdub G. Ali[1], Francis B. Dejene[1]*, Hendrik C. Swart[2]

1 *Department of Physics, University of the Free State (Qwaqwa Campus), Private Bag X13, Phuthaditjhaba, 9866, South Africa*

2 *Department of Physics, University of the Free State, P.O. Box 339, Bloemfontein, 9300, South Africa*

Received 09 April 2011; accepted 09 November 2011

Abstract: Un-doped and Mn-doped ZnO nanoparticles were successfully synthesized in an ethanolic solution by using a sol-gel method. Material properties of the samples dependence on preparation conditions and Mn concentrations were investigated while other parameters were controlled to ensure reproducibility. It was observed that the structural properties, particle size, band gap, photoluminescence intensity and wavelength of maximum intensity were influenced by the amount of Mn ions present in the precursor. The XRD spectra for ZnO nanoparticles show the entire peaks corresponding to the various planes of wurtzite ZnO, indicating a single phase. The diffraction peaks of doped samples are slightly shifted to lower angles with an increase in the Mn ion concentration, signifying the expansion of the lattice constants and increase in the band gap of ZnO. All the samples show the absorption in the visible region. The absorbance spectra show that the excitonic absorption peak shifts towards the lower wavelength side with the Mn-doped ZnO nanoparticles. The PL spectra of undoped ZnO consist of UV emission at 388 nm and broad visible emission at 560 nm with varying relative peak intensities. The doping of ZnO with Mn quenches significantly the green emission while UV luminescence is slightly affected.

PACS (2008): 78.55.-m; 78.67.-n

Keywords: ZnO:Mn • nanoparticles • Wurtzite • absorption • Crystalline • photoluminescence

1. Introduction

Zinc oxide nanostructures are semiconducting inorganic nanocrystallites with dimensions less than 100 nm, in one or more dimensions. Consequently, discrete electronic states, unusual structural transformations, unique optical properties and a blue shift of the band edge transition energy are induced in these nanoparticles [1, 2]. Due to high surface-to-volume ratio, the surface atoms play a large role in the properties of nanomaterials, which usually have fewer adjacent coordinate atoms and can be treated as defects as compared with the bulk atoms. These defects induce additional electronic states in the band gap, which can mix with the intrinsic states to a substantial extent and which may influence the spacing of the energy levels and the optical properties of nanopowders. Thus, nanoparti-

*E-mail: dejenebf@qwa.ufs.ac.za

cles especially quantum dots (QDs) exhibit unique properties and have a broad range of applications in optoelectronics, telecommunications, lasers and optical sensors [3–5]. Therefore, simple synthesis routes for ZnO nanoparticles with a diameter less than or comparable to QDs which is below 7 nm [4] for zinc oxide are extremely important in materials research. ZnO is an important commonly n-type wide-energy-gap semiconductor (Eg = 3.37 eV, 330 K) which has a wide range of applications such as in solid-state gas sensors, transparent conducting electrodes, and optical electronic devices [6–10]. Among various methods, sol-gel is well suited for production of nanostructured materials, because of its relatively low processing cost and the ability to control the grain size. In this study, a simple sol-gel route for synthesizing of wide-dispersed ZnO nanostructures within a small diameter range 6 to 20 nm. The novelty of this work is the use of small mole% of Mn ions as do-pants which lead to fabrication of different shapes and structures of ZnO:Mn nanostructures without using of any surfactant or other additives. Doped ZnO materials are of technological importance because of their great potential for applications in optoelectronic devices and luminescent materials [11, 12]. Generally, ZnO exhibits two kinds of emissions: one is an ultraviolet (UV) near-band-edge emission at approximately 380 nm and the other a visible deep-level emission with a peak anywhere in the range from 450 to 730 nm [13, 14]. The visible emissions are related to intrinsic defects or dopants in the ZnO crystal and depend greatly on the preparation methods and conditions. For example, red luminescence can be observed in ZnO doped with Li, Na, N, P, Ne, or Bi [15–17]. However, visible luminescence (except green) has relatively low intensity and its origin remains unclear. Recently, Mn-doped ZnO materials have attracted much attention because of their excellent ferromagnetic properties [18] and unique UV-luminescent properties based on radiative recombination of the electron-hole pairs [19, 20]. Doping Mn into ZnO offers an interesting way to alter various properties [21, 22], for example the band gap of host material can be tuned from 3.37 eV to 3.70 eV. Also it alters the emission properties by providing an efficient channel for the recombination of electron and hole via the do-pant Mn d levels. By varying the size of particles below 10 nm, optical and electronic properties can further be tuned.

2. Experimental details

Colloidal solution was prepared from zinc acetate and absolute ethanol. 0.918 g of zinc acetate was dissolved in 60 ml of absolute ethanol (99.999%) and vigorously stirred for 30 minutes at 70°C. Different mole ratios of manganese acetate was dissolved in 10 ml of absolute ethanol and added drop wise to Zn^{2+} solution under vigorous magnetic stirring. 0.55 g NaOH was separately dissolved in 20 ml of similar ethanol and stirred in a preheated ultrasonic bath for one hour. This was slowly added to the solution while stirring in ice-water. Stirring ran for 24 hrs and a brownish colloidal solution was washed in a mixture of ethanol and heptane repeatedly. It was then kept in a fume chamber for 2 days to dry. The X-ray diffraction (XRD) patterns were recorded to characterize the phase and crystal structure of the nanoparticles using a multi-purpose XRD system with a Siemens Diffractometer D5000 with a CuK_{α} radiation source at 40 kV, 30 mA and $\lambda = 1.5418$ Å. The morphology of the nanoparticles was observed by a Shimadzu Superscan SSX-550 system scanning electron microscope (SEM) operated at 20 kV equipped with energy dispersive X-ray spectroscopy (EDS). Optical absorption was performed on an Agilent HP1100 diode-array UV-visible spectrophotometer. Room temperature photoluminescence (PL) of the samples was measured, using a He-Cd laser (325 nm) as excitation sources.

3. Results and discussion

3.1. Morphological and structural properties

Surface morphological studies of the undoped and Mn-doped ZnO have been carried out using scanning electron micrographs Fig. 2a-b shows the SEM images of undoped and a representative of Mn-doped ZnO (Mn 2.5%) powders. SEM photograph of pure ZnO (Fig. 2a) shows large, agglomerated, roughly spherical nanoparticles and nearly smooth morphology. The Mn doped ZnO micrograph (Fig. 2b) depict nanorods network surface morphology.

The formation of many long nanosize rods all over the surface are attributed to the presence of the Mn ions. The Mn atoms may have disturbed the growth process by acting as a seed, resulting in the formation of nanosize rods. The increase in manganese concentrations seems to increase the radius of the cylindrical nanorods formed. Therefore the incorporation of Mn at the Zn site was found to influence the surface morphology of the powders. It is interesting to note that the grain sizes observed from SEM is significantly different from the grain size determined from using XRD measurements. This shows the grains seen in the SEM are the domains formed by aggregation of nanosize crystallites [23]. Energy dispersive x-ray analysis showed that the amount of Mn element in the sample increased depending on the increasing Mn incorporation in the solution. As a result, Mn incorporation has a strong effect

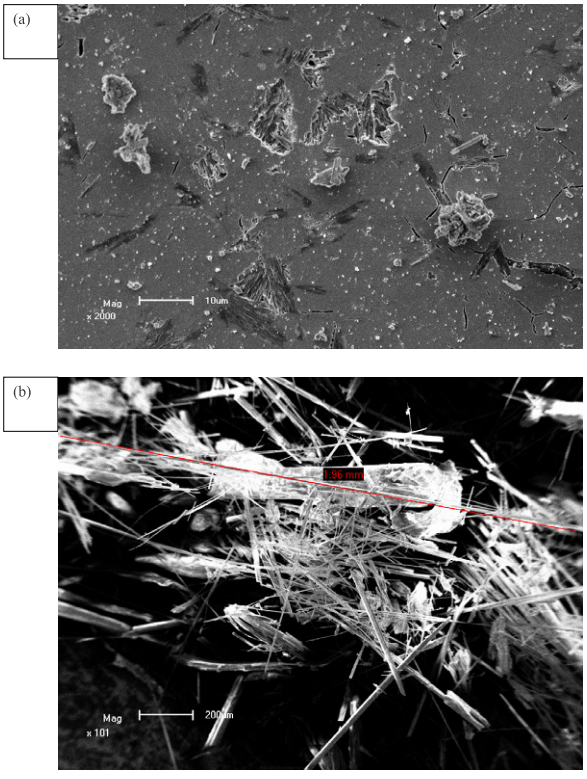

Figure 2. Graphs of (a) undoped ZnO and (b) a representative of Mn-doped ZnO nanorods.

on the optical, structural and morphological properties of ZnO. The Energy dispersive x-ray analysis shown in Fig. 3 consists of Zn and O and confirms the presence of Mn in the ZnO particles with wt% less than the nominal value of Mn in ZnO (Note: traces of C less than 0.1 wt% are also observed). Manganese is different from other transition metals when substituted in an $A^{II}B^{VI}$ matrix, since it forms stable phases over a wide range of compositions.

It appears that the ease with which the manganese substitutes for the group II elements in the zinc-blende and wurtzite structures results from the fact that the 3d orbitals of Mn are exactly half-filled. Figures 4 are representative XRD patterns taken from the undoped and Mn doped ZnO nanoparticles prepared by sol-gel technique. The superior structural properties of the reference nanostructures are clearly reflected by the XRD results. In general, these particles were characterized by sharp, well-defined peaks with no preferred orientation. Strongly pronounced peaks, <100>, <002> and <101> appear at $2\theta = 31.43$, 34.13 and 35.93 respectively, which indicate that the samples are polycrystalline. Few weaker peaks can also be seen in Mn-doped sample in the XRD pattern. These few peaks may be assigned to Mn_3O_4. That is to say, not all

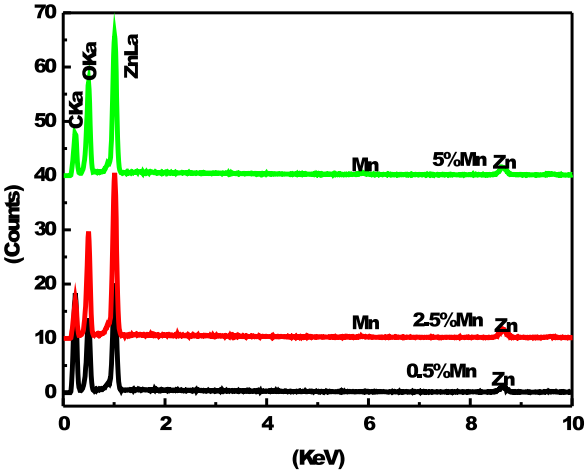

Figure 3. EDS analysis.

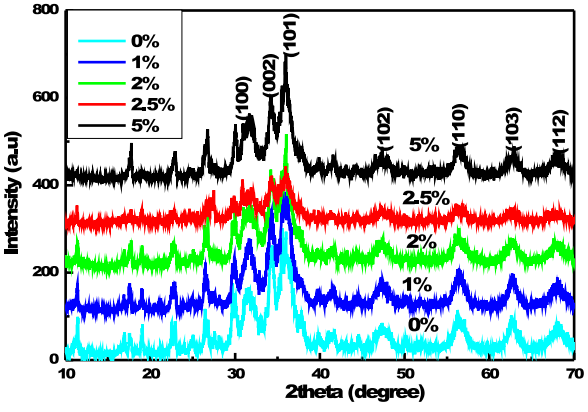

Figure 4. XRD pattern of ZnO: Mn with various concentration of mn^{2+}.

the stoichiometric Mn^{2+} has entered the ZnO lattice, the rest of Mn^{2+} has been oxidized into manganese oxide. Ivill et al. [24] has also reported the precipitation of Mn_3O_4 in $Zn_{1-x}Mn_xO$ powder deposited on sapphire by pulsed laser deposition (PLD) at the Mn concentration of 3 at%. Samples were randomly orientated along different planes, the "d" value were compared with standard JCPDS data card (79-0207) which confirms the wurtzite structure of the materials. Crystallite size of the ZnO powder samples was calculated from the peaks width using Debye-Scherer formula;

$$D = (0.9\lambda)/(\beta_{1/2}cos\theta). \quad (1)$$

Where, D is the diameter of the crystallites, λ is the wavelength of Cu K_α line, θ is the Bragg's angle and β is full

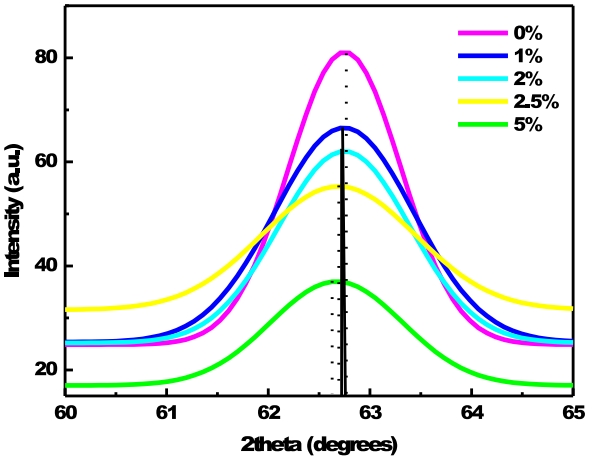

Figure 5. XRD spectra of doped and undoped ZnO powders at single plane, i.e. <110>.

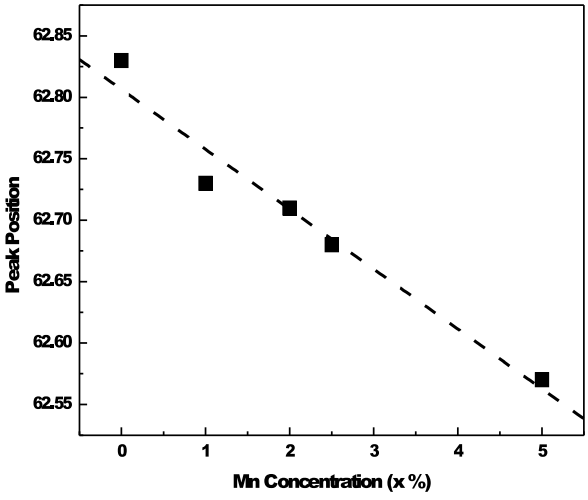

Figure 6. Variation of <112> peak position with Mn mole% concentrations.

width at half maximum (FWHM). The calculated particle sizes of un-doped and Mn doped samples were obtained in the range of 5 - 7 nm as tabulated in Table 1.

The peaks (especially high angle peaks) of the diffraction patterns of doped samples are slightly shifted to lower angles with an increase in Mn molar ratio (see Fig. 5). Fig. 6 show an approximately linear relation between the <110> peak position and the amount of mol% of Mn^{2+} ions present in the sample. This means that small variation in the lattice parameters occur as Mn^{2+} concentration in the sample increases. The lattice constants of Mn doped ZnO obtained by least square method, shown in Table 2 were slightly larger than those of undoped ZnO, because the ionic radius of Mn (II) (0.66) is slightly larger than that of Zn (II) (0.60) [20]. The length of both *a* and *c* axis expand slightly with the increasing Mn^{2+} doping in ZnO. The expansion of the lattice constants (Table 2) and the slight shift of XRD peaks with an increase in concentration of Mn doped ZnO indicated that manganese has really doped into the ZnO structure.

The average ratio *c*/*a* of Mn-doped ZnO is approximately 1.600, which is slightly less than that of pure ZnO (1.604). This value is related to the positional '*u*' parameter in the wurtzite structure and the Zn-O bond length *l* is calculated using the '*u*' parameter. The Zn-O bond lengths calculated for pure ZnO and Mn-doped ZnO powders from FTIR measurements are 1.9758 and 1.9762 Å, respectively. The interplanar spacing has been increased due to a slight shift in 2θ for the Mn-doped powder, which is consistent with Zn-O length. Substitution of Mn^{2+} for Zn^{2+} requires a local expansion of the lattice to accommodate the manganese ion due to ionic radii difference. This induces higher covalent bonding for the Mn^{2+} substitutes in ZnO: Mn, which is in agreement with the bond length determined.

3.2. Optical properties

3.2.1. Transmission and absorbance

Optical absorption spectra of the undoped and Mn- doped ZnO powder recorded in the wavelength region of 200-850 nm is shown in Fig. 7. The absorbance is found to be a minimum for undoped ZnO powders and increases with an increase in mole Mn%. The decrease in optical absorption is associated with the loss of light due to (i) oxygen vacancies and (ii) scattering at grain boundaries. A characteristic difference in the absorption edge was observed with Mn incorporation in ZnO. A sharp absorption edge has been observed for undoped ZnO while Mn-doped display slightly lesser sharp drop in absorption edge. This implies slight difference in size distribution of the monodispersed nature of the nanoparticles between pure and doped samples. It is clearly visible from absorbance spectra that the excitonic absorption peak shifts towards the lower wavelength side with the Mn-doped ZnO nanoparticles. This values lie much below the bandgap wavelength of 375 nm (E_g = 3.3 eV) of bulk ZnO [25]. The relatively high absorbance at longer wavelengths and broad absorption edge for doped ZnO indicates large dispersion in size of the ZnO:Mn nanostructures and their arbitrary orientations. The position of the absorption band is observed to shift towards the lower wavelength side with the Mn-doped ZnO nanoparticles. This confirms the XRD findings that the band gap of ZnO material changes with the doping concentration of Mn^{2+} ion. Similar ob-

Table 1. Average particle size as a function of mol% Mn^{2+}.

$Zn_{1-x}Mn_xO$ composition	Average grain size as function of mol.% Mn^{2+} in ZnO				
	<102>	<110>	<103>	<112>	Grain size
ZnO	6.7	7.0	7.0	6.6	6.8
$Zn_{0,99}Mn_{.0.01}O$	6.1	7.0	7.0	6.2	6.6
$Zn_{0,98}Mn_{.0.02}O$	5.4	6.8	6.9	5.9	6.3
$Zn_{0,975}Mn_{.0.025}O$	5.2	6.4	6.9	5.7	6.1
$Zn_{0,95}Mn_{.0.05}O$	5.9	7.4	7.1	5.6	6.5
	Average grain size				6.46±0.12

Table 2. Lattice constants of undoped and Mn-doped ZnO nanoparticles.

$Zn_{1-x}Mn_xO$ composition	Lattice parameter		
	a	b	c/a
ZnO	3.246	5.208	1.604
$Zn_{0.99}Mn_{0.01}O$	3.265	5.221	1.599
$Zn_{0.92}Mn_{0.02}O$	3.270	5.237	1.601
$Zn_{0.975}Mn_{0.025}O$	3.279	5.245	1.599

servation of enhancement of the band gap of ZnO with Mn^{2+} ion concentration was also made earlier by Mandal and Nath and Fukumura et al. [26, 27]. The crystalline grain sizes of 1%, 3%, 5%, and 10% Mn doped ZnO samples were calculated by the phonon confinement model as 31.8, 18.3, 15.9, and 14.1 nm, respectively by Samanta et al. [28]. The group found that the optical band gap increased from 3.27-3.41 eV due to the Mn doping. The increase in band gap from bulk ZnO with dopant concentration (x) can be attributed to the sp-d spin exchange interaction between the band electrons and localized spin of the transition metal ions [27]. It is clear that the ZnO nano particles doped with Mn have an excellent absorbing UV ray capability. The relationship between the optical absorption coefficient (α) and the incident photon energy ($h\upsilon$) from the optical absorption measurements for a direct band-gap material is given by

$$(\alpha h\upsilon)^2 \sim (h\upsilon - Eg). \quad (2)$$

Using this information, graphs of $(\alpha h\upsilon)^2$ were plotted against $h\upsilon$ and the linear region was extrapolated to $(\alpha h\upsilon)^2 = 0$ to give a value of the optical energy gap. Fig. 8 displays the band-gap variation of the ZnO:Mn nanostructures as a function of manganese concentrations. The plot of experimental values of optical band gap for ZnO powders with varying manganese content are shown in Fig. 9.

The calculated average optical band gap for all prepared ZnO powders was 3.79 ± 0.23 eV. The band gap values slightly increases to approximately 3.92 eV with an increase in Mn concentration but for Mn molar fraction of

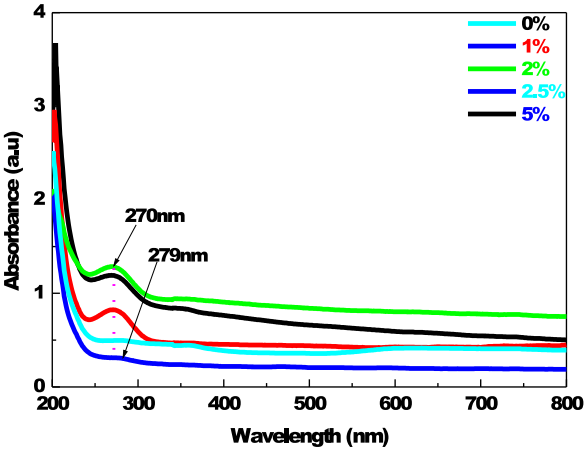

Figure 7. UV-vis absorption spectra of undoped and doped ZnO nanoparticles.

5% correlation does not hold, this could imply that Mn ions are not fully in cooperated into ZnO lattices.

3.3. Photoluminescence properties

The PL spectra of undoped ZnO consist of UV emission at 388 nm and broad visible emission at 560 nm with varying relative peaks intensity. Generally, the UV emission is attributed to the exciton radiative recombination while that of the visible emission has been attributed to defects. The PL exciton emission is observed at a slightly red-shift wavelength in respect to the absorption onset. Sakohara et al. found that the shift of wavelength is re-

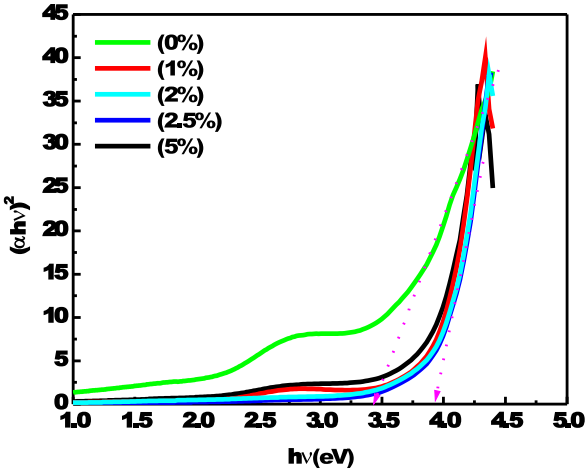

Figure 8. Graph of $(\alpha h\upsilon)^2$ vs $h\upsilon$ for different concentrations of manganese in ZnO:Mn nanoparticles.

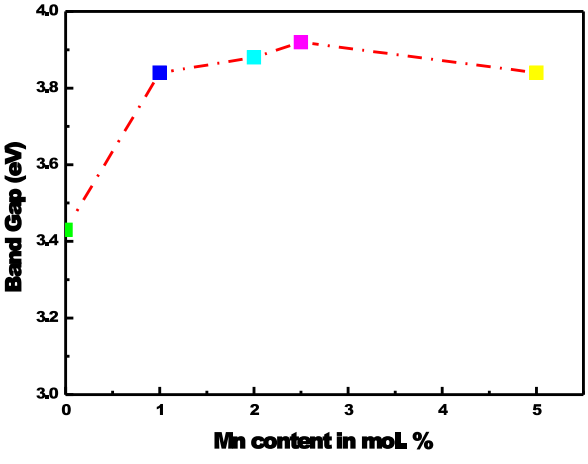

Figure 9. Band Gap for ZnO:Mn nano powders with the Mn concentration varied between 0, 1.0, 2.0, 2.5 and 5.0 at.%.

lated to the ZnAc/LiOH ratio [29]. Some models have been proposed to explain this red-shifted emission. One common origin is the electron-phonon interaction [30]. In nanocrystals, because the lattice reorganization is related to the electron-hole density and because quantum confinement enhances the density, the shift will be enhanced substantially. The size distribution in our samples adds an extrinsic contribution to the red shift. Defects in ZnO strongly depend on the preparation, annealing conditions and do-pants which in turn affect the photoluminescence properties. In this study the large concentration of defects in the ZnO nanostructures prepared at low temperatures can be controlled by doping with different concentration of Mn^{2+} ions. In the past 40 years, various mechanisms have been proposed [31–33]. Until recently, Dijken et

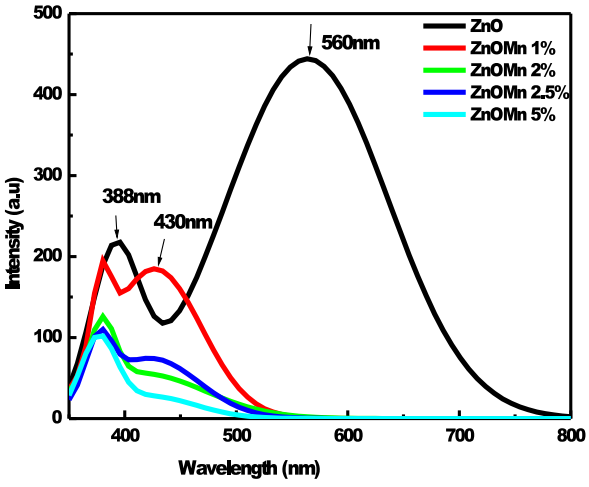

Figure 10. Fluorescence spectra (obtained with λext =325 nm) of ZnO and Mn-doped ZnO with various concentration of Mn.

al. figured that the particle surface played an important role in the visible emission [34]. They offered a model: The valence band hole can be trapped by surface states and then tunnels back into oxygen vacancies containing one electron (V^{+}_{O}) to form V^{++}_{O} recombination center. The recombination of a shallowly trapped electron with a deeply trapped hole in a V^{++}_{O} center causes visible emission. The transitions from surface traps to deep level defects are significantly quenched on doping with Mn ions, as indicated by a marked reduction of emission feature at 560 nm. It is clear from the graph (Fig. 10) that doping of ZnO with Mn quenches significantly both the green emission as well as the UV luminescence. The 1 % Mn sample display enhanced luminescence at 430 nm completely different from all other samples. This is possibly due to the emission from the Mn ions at octahedron sites. The Mn^{2+} ions emission at 430 nm was found not to be proportionally dependent on the concentration of Mn^{2+} ions present. The difference in influence of Mn^{2+} ions on the UV and visible emissions when optimized has potential for the applications of doped ZnO to be used in UV sensors.

4. Conclusions

Undoped ZnO nanoparticles and Mn doped ZnO nanorods having nanometer sized width and micrometer-sized lengths were synthesized in the laboratory using the sol-gel technique. SEM images show nanorods morphology for doped ZnO. XRD patterns confirm the polycrystalline wurtzite structure of ZnO. Mn doped nanorods have sev-

eral applications as the best suited materials for sensors, spintronics, high energy density batteries, better insulation materials etc. Photoluminescence spectra of the undoped ZnO are composed of two main emission bands peaked at 388 nm and 560 nm. Doping ZnO with Mn^{2+} quenches significantly the green emission and slightly the yellow one. At room temperature, the super-radiation phenomena of the UV photoluminescence seems to be produced at only high density excitation, therefore the UV emissions are ascribed to intrinsic exciton photoluminescence. However, green band probably originates from the defect related to oxygen.

References

[1] F. C. M. Van De Pol, Ceramics Bulletin. 69 (1990) 1959
[2] K. Nashimoto, S. Nakamura, H. Mariyama, Jpn. J. Appl. Phys. 43, 5091 (1995)
[3] T. Nagata, T. Shimura, A. Asida, N. Fujimura T. Ito, J. Cryst. Growth 237, 537 (2002)
[4] A. J. Freeman, K. R. Paeppelmeier, T. O. Mason, R. P. H. Chang T. J. Marks, Mater. Res. Soc. Bull. 25, 45 (2000)
[5] L. Spanhel, M. A. Anderson, J. Am. Chem. Soc. 113, 2826 (1991)
[6] X. Wu et al., Appl. Phys. Lett. 85, 3657 (2004)
[7] N. F. Cooray et al., Jpn. J. Appl. Phys. 38, 6213 (1999)
[8] Y. J. Xing et al., Appl. Phys. Lett. 83, 1689 (2003)
[9] W. Shan et al., Appl. Phys. Lett. 86, 153117 (2005)
[10] Z. W. Jin et al., Appl. Phys. Lett. 83, 39 (2003)
[11] B. S. Jeon, J. S. Yoo, J. D. Lee, J. Electrochem. Soc. 143, 3923 (1996)
[12] Y. Nakanishi et al., Appl. Surf. Sci. 142, 233 (1999)
[13] K. Vanheusden et al., Appl. Phys. Lett. 68, 403 (1996)
[14] R. M. Nyffenegger, B. Craft, M. Shaaban, S. Gorer, G. Erley, R. M. Penner, Chem. Mater. 10, 1120 (1998)
[15] O. F. Schirmer, D. Zwingel, Solid State Commun. 8, 1559 (1970)
[16] B. J. Pierce, R. L. Hengehold, J. Appl. Phys. 47, 644 (1976)
[17] J. A. Garcia, A. Remon, J. Piqueras, J. Appl. Phys. 62, 3058 (1987)
[18] N. H. Hong, J. Sakai, V. Brize, J. Phys. Condens. Mat. 19, 036219 (2007)
[19] T. Makino et al., Appl. Phys. Lett. 81, 2355 (2002)
[20] W. M. Hlaing Oo, L. V. Saraf, M. H. Engelhard, V. Shutthanandan, L. Bergman, J. Huso, M. D. McCluskey, J. Appl. Phys. 105, 013715 (2009)
[21] H.-J. Lee, S.-Y. Jeong, C. R. Cho, C. H. Park, Appl. Phys. Lett. 81, 4020 (2002)
[22] G. Srinivasan, J. Kumar, Cryst. Res. Technol. 41, 893 (2006)
[23] K. Nashimoto, S. Nakamura, H. Mariyama, Japan. J. Appl. Phys. 43, 5091 (1995)
[24] M. Ivill, S. J. Pearton, D. P. Norton, J. Appl. Phys. 97, 053904 (2005)
[25] S. Sakohara, M. Ishida, M. A. Anderson, J. Am. Chem. B 102, 10169 (1998)
[26] T. Fukumura et al., Appl. Phys. Lett. 78, 958 (2001)
[27] S. K. Mandal, T. K. Nath, Thin Solid Films 515, 2535 (2006)
[28] K. Samanta, S. Dussan, R. S. Katiyar, P. Bhattacharya, Appl. Phys. Lett. 90, 261903 (2007)
[29] S. Sakohara, M. Ishida, M. A. Anderson, J. Phys. Chem. B 102, 10169 (1998)
[30] M. Lannoo, C. Delerue, G. Allan, J. Lumin. 70, 170 (1996)
[31] K. Vanheusden, W. L. Warren, C. H. Seager, D. R. Tallar, J. A. Voigt, B. E. Gnade, J. Appl. Phys. 79, 7983 (1996)
[32] Y. Li, G. W. Meng, L. D. Zhang, F. Phillipp, Appl. Phys. Lett. 76, 2011 (2000)
[33] S. A. Studenilin, N. Golego, M. Cocivera, J. Appl. Phys. 84, 2287 (1997)
[34] A. van Dijken, E. A. Meulenkamp, D. Vanmaekelbergh, A. Meijerink, J. Phys. Chem. B 104, 1715 (2000)